Computer simulation study of free energy barriers in crystal nucleation

J. S. van Duijneveldt
Van 't Hoff Laboratory, University of Utrecht, Padualaan 8, 3584 CH Utrecht, The Netherlands

D. Frenkel
FOM Institute for Atomic and Molecular Physics, Kruislaan 407, 1098 SJ Amsterdam, The Netherlands

(Received 2 July 1991; accepted 29 November 1991)

We show how relatively standard Monte Carlo techniques can be used to probe the free-energy barrier that separates the crystalline phase from the supercooled liquid. As an illustration, we apply our approach to a system of soft, repulsive spheres $[v(r) = \epsilon(\sigma/r)^{12}]$. This system is known to have a stable face-centered-cubic (fcc) crystal structure up to the melting temperature. However, in our simulations, we find that there is a surprisingly low free-energy barrier for the formation of body-centered-cubic (bcc) crystallites from the melt. In contrast, there appears to be no 'easy' path from the melt to the (stable) fcc phase. These observations shed new light on the results of previous simulations that studied the *dynamics* of crystal nucleation in the r^{-12} system. We argue that the techniques developed in this paper can be used to gain insight in the process of homogeneous nucleation under conditions where direct, dynamical simulations are inconclusive or prohibitively expensive.

I. INTRODUCTION

Computer simulation studies have contributed considerably to our understanding of the freezing transition. In 1957, Alder and Wainwright[1] and Wood and Jacobson[2] showed that a system of purely repulsive hard spheres can undergo a first-order transition from the fluid to the crystalline state. Some 10 years later, Hoover and Ree showed how computer simulations can be used to locate the freezing point of an arbitrary 'atomic' fluid.[3] Subsequently, simulations have been used to determine both the freezing point and the structure of the solid at freezing for a wide range of interatomic potentials (see, e.g., Refs. 4–6). In particular, Hoover *et al.*[7] investigated the stability of different crystalline phases for a class of model systems with repulsive pair interactions of the form $v(r) = \epsilon(\sigma/r)^n$. This study showed that for $n \geqslant 7$, the stable crystal structure at melting is face centered cubic (fcc), whereas at lower values of n, the solid melts from the body-centered-cubic (bcc) phase. In other words, 'hard' repulsive interactions favor fcc solids, while bcc occurs for 'soft' interactions.

In the mid-seventies, computer simulations were first used to study the *dynamics* of crystallization, rather than the thermodynamics. Starting with the work of Mandell *et al.*,[8] a large number of numerical simulations of the homogeneous nucleation process have been reported.[9-24] For a review, see, e.g., Refs. 25 and 26.

Computer studies of the dynamics of homogeneous crystallization are much less straightforward than the numerical determination of the fluid–solid coexistence point. Below, we list some of the factors that make computer-simulations studies of crystallization time consuming and, in many cases, difficult to interpret.

Let us first briefly recall the usual approach to study crystallization in a computer 'experiment.' In such a molecular dynamics (MD) simulation, the system is first prepared in a stable, well-equilibrated fluid phase. The temperature of this fluid is then rapidly quenched to a value well below the freezing point (T_f) (often as low as $0.5T_f$, or even lower). The system is then allowed to evolve. During this time evolution one monitors a number of dynamical observables (e.g., the pressure, or the structure factor) that can be used to detect the onset of homogeneous nucleation.

This procedure has a number of practical drawbacks. First of all, the system size appears to have a large effect on the rate of nucleation. The size of the critical nucleus and the time of formation of a critical nucleus are smaller in a small system than in a large system.[13,27] Recently, Swope and Andersen have reported a simulation study of homogeneous nucleation in a very large system (10^6 particles). This study indicates that system-size effects become unimportant only for model systems containing more than 10^4 particles. Such a system size is a factor 10–50 larger than what is typically needed to study equilibrium properties of dense fluids. As a consequence, nucleation studies tend to be computationally expensive.

This problem is compounded by the fact that it may take a long time (and therefore a lot of computer time) before a nucleation event is observed, unless the fluid is strongly supercooled. How much supercooling is needed to achieve a reasonable rate of nucleation (on the time scale of a computer 'experiment'), depends strongly on the harshness of the interatomic potential. Mountain *et al.*[20] have performed simulation studies of crystal nucleation in two soft-sphere systems $[v(r) \sim r^{-n}$, with $n = 7$ and $n = 12]$ and in a Lennard-Jones system. They observed that nucleation and growth take place more easily as the interaction between particles becomes softer. A similar conclusion was reached by Robbins *et al.*[21] who studied crystal nucleation in a Yukawa fluid. The strong dependence of the nucleation rate on the harshness of the short-range repulsion between atoms can be understood intuitively by noting that soft spheres will slip more easily into a new position than densely packed hard

spheres. Experimentally, the same correlation between nucleation rate and the softness of the intermolecular potential has been observed in a study of the formation of colloidal crystals.[28]

In order to see homogeneous crystal nucleation in a computer simulation, the initial fluid phase must be supercooled to a temperature that is far below the equilibrium freezing temperature. This is true for fluids with a 'soft' intermolecular potential, but even more so for the more harshly repulsive systems (i.e., those systems that tend to form stable fcc crystals). Unfortunately, it is not known *a priori* if crystal nucleation at such extreme supercooling proceeds in the same way as crystallization close to the freezing temperature. This fact severely limits the use of MD studies to investigate whether nucleation proceeds directly into the thermodynamically stable phase or that a metastable solid phase is formed first, in accordance with Ostwald's 'step rule'.[29] The latter rule states that the crystal structure that is nucleated from the melt does not correspond to the most stable phase, but to the phase that is nearest (in free energy) to the fluid phase. A closely related rule is the one due Stranski and Totomanow,[30] who argue that the crystal phase that forms first is the one with the lowest free energy barrier for nucleation. One of the aims of the early work of Mandell *et al.*[9] was precisely to test whether Ostwald's rule applied to the homogeneous crystallization of the Lennard-Jones fluid. In Ref. 9 evidence was presented that indicated the formation of bcc nuclei in a small, strongly supercooled Lennard-Jones (LJ) system. However, all other studies of the same system found evidence for the formation of fcc nuclei.[10,8,14] In particular, the recent numerical study by Swope and Andersen[16] of crystal nucleation in a system of 10^6 LJ particles, shows convincingly that, although both bcc and fcc nuclei can form under conditions of strong supercooling, only the fcc nuclei (i.e., the ones that correspond to the thermodynamically stable phase) grow to form larger crystallites. In contrast, numerical studies of homogeneous nucleation in (considerably smaller) r^{-12}-'soft-sphere' systems[18,19] indicate that, although fcc is the thermodynamically stable crystal phase, bcc crystallites tend to form even at large supercooling. This observation is in qualitative agreement with the theoretical predictions of Alexander and McTague[31] who argue that, at least for small supercooling, nucleation of bcc crystallites should be favored in all simple fluids that have a 'weak' first-order freezing transition. A recent theoretical study by Klein and Leyvraz[32] supports the idea that a metastable bcc phase should nucleate relatively easily from the melt. Experimentally, nucleation of a metastable bcc phase has been observed in rapidly cooled metal melts.[33]

Clearly, it would be desirable to have a numerical technique that allows us to study crystal nucleation at temperatures closer to the coexistence point. The straightforward MD approach will not work under those conditions because the rate of nucleation depends exponentially on the degree of supercooling. A mildly supercooled fluid will never crystallize during a molecular dynamics simulation. In the present paper we do not attempt to solve the full problem of crystal nucleation close to coexistence. Rather, we exploit the fact that nucleation is an *activated* process and that the rate of nucleation can therefore be considered as the product of two terms, namely, (1) the probability to find the system at the top of the free-energy barrier to nucleation and (2) the rate at which this 'activated' state transforms into a stable crystallite. Below, we show how relatively simple computer-simulation techniques can be used to gain information about the free-energy barrier to nucleation. We shall not discuss the second factor, although we stress that the techniques described in the present paper could be used to prepare a slightly supercooled fluid at the top of the free-energy barrier. The standard techniques to compute chemical reaction constants[34,35] could then be used to compute the actual rate of nucleation.

The central problem in determining the nucleation barrier is that the 'reaction coordinate' from fluid to crystal is not known *a priori*. Moreover, we do not wish to impose any specific reaction path (e.g., one leading from the fluid to only one of all the possible crystal phases). Rather, we wish to use as our reaction coordinate any order parameter Φ that is sensitive to the overall degree of crystallinity in the system but much less sensitive to the differences between the possible crystal structures. Below we show that it is indeed possible to define such an 'unbiased' reaction coordinate.

The Helmholtz free energy of the system, F, is a function of this order parameter. In fact, it follows from equilibrium statistical mechanics[36] that

$$F(\Phi) = \text{constant} - k_B T \ln\{P(\Phi)\}, \tag{1}$$

where $P(\Phi)$ is the probability per unit interval to find the order parameter around a given value of Φ. We expect that above the freezing temperature, $P(\Phi)$ will be strongly peaked at a low (liquidlike) value of Φ. Close to coexistence, $P(\Phi)$ should develop a double-peaked structure. The second peak corresponds to a solidlike value of Φ. In between these two peaks, $P(\Phi)$ will be very small, but finite. From Eq. (1) we obtain our estimate for the barrier to nucleation from the minimum value of $P(\Phi)$ between the solidlike and the liquidlike peak.

As $P(\Phi)$ is an equilibrium property of the system under consideration, it can, in principle, be probed both by Monte Carlo and by molecular dynamics simulations. However, in an ordinary simulation, the system will spend almost all its time in either the liquid or the solid state and it will therefore be impossible to obtain good statistics on $P(\Phi)$ for intermediate values of the order parameter. We circumvent this problem by using a non-Boltzmann Monte Carlo sampling scheme, namely, the 'umbrella sampling' technique of Torrie and Valleau.[37] Using this technique, we are able to measure $F(\Phi)$ as a function of the crystallinity Φ. Moreover, we obtain information about the structure of the solid phase at the other side of the barrier. Below we show that, at least for the r^{-12} system, the solid phase that is reached from the fluid by crossing the lowest free-energy barrier is, in fact, not the equilibrium fcc phase but the bcc phase.

The rest of this paper is organized as follows. In Sec. II we briefly summarize the umbrella sampling technique. In Sec. III, we discuss our choice for the crystallinity order parameter. The computational details are summarized in Sec. IV. Section V contains our results for the nucleation

barriers in the r^{-12} system and in Sec. VI we discuss some of the implications of the present work.

II. UMBRELLA SAMPLING

As indicated in the previous section, special numerical techniques are required to sample the equilibrium distribution function $P(\Phi)$. There exist two closely related techniques to measure such distribution functions. One is based on a dynamical determination of the force conjugate to the 'reaction coordinate' Φ.[35] Such a calculation requires a series of MD simulations at different fixed values of Φ. In our case, where the order parameter happens to be defined as a discontinuous function of the atomic coordinates (see Sec. III), this 'constraint' method is less attractive. We have therefore used the umbrella-sampling technique of Torrie and Valleau[37] to measure $P(\Phi)$. The basic idea behind this method is to bias the Monte Carlo sampling of configuration space in such a way that points high on the free-energy barrier are sampled frequently. In order to compute $P(\Phi)$, we must correct for our sampling bias. Below, we briefly summarize how this is achieved in practice.

Consider a Monte Carlo simulation in the canonical (NVT) ensemble. The average of a quantity A which depends on the atomic coordinates q^N is given by

$$\langle A \rangle_{NVT} = \int dq^N A(q^N) \exp(-\beta \mathscr{V}(q^N)) \int dq^N \exp(-\beta \mathscr{V}(q^N)), \tag{2}$$

where $\mathscr{V}(q^N)$ is the potential energy function and $\beta \equiv 1/k_B T$. The umbrella sampling scheme was devised to handle situations where important contributions to $\langle A \rangle$ come from configurations for which the Boltzmann factor $\exp(-\beta \mathscr{V})$ is small, in which case Eq. (2) yields poor statistics. The umbrella sampling scheme is based on the fact that Eq. (2) can be rewritten as

$$\langle A \rangle_{NVT} = \int dq^N w^{-1}(q^N) A(q^N) \exp(-\beta \mathscr{V}(q^N)) w(q^N) \int dq^N w^{-1}(q^N) \exp(-\beta \mathscr{V}(q^N)) w(q^N), \tag{3}$$

where w is an, as yet unspecified weight function. Rather than perform a Monte Carlo sampling of the original (Boltzmann) distribution function, we now consider configurational averages obtained by sampling according to the biased distribution function $\exp(-\beta \mathscr{V}) w$. We label averages in the original and biased 'ensembles' with the subscripts 0 and w, respectively,

$$\langle A \rangle_0 = \frac{\langle A/w \rangle_w}{\langle 1/w \rangle_w} = \langle A/w \rangle_w \langle w \rangle_0. \tag{4}$$

The right-hand side of Eq. (4) shows that, in order to obtain good statistics for $\langle A \rangle_0$, the biased distribution function $\exp(-\beta \mathscr{V}) w$ should overlap with A/w, while w itself must overlap with $\exp(-\beta \mathscr{V})$. *This 'bridging' nature of* w explains the name 'umbrella sampling.'

Finally, we have to decide on a suitable form for w. In general, this choice will depend on the region in configuration space that contributes most to the desired average $\langle A \rangle$. In the present case $\langle A \rangle$ corresponds to the probability distribution function $P(\Phi)$ of some order parameter Φ:

$$P(\Phi) = \langle \delta(\Phi - \Phi(q^N)) \rangle. \tag{5}$$

We are interested in the free-energy barrier $F(\Phi)$ [see Eq. (1)]. The minima of this free energy occur at values of Φ that correspond to homogeneous phases. When the system moves from one phase to another, F will go through a maximum. Clearly, we should construct a biasing function w that allows us to probe $P(\Phi)$ over the entire free-energy barrier.

The optimum choice for w would be $w = \exp(+\beta F(\Phi))$, because in that case the biased distribution function would be flat, i.e., all values of Φ are sampled with the same frequency. However, this choice of w requires the final answer of the calculation as input. In practice, we first perform a simulation without any weighting function. This yields a local estimate for $F(\Phi)$. Next, the simulation is repeated using the current estimate for $F(\Phi)$ to construct the biasing function $w \approx \exp(\beta F)$. At first sight, it might seem advantageous to refine the computation of w in such a way that *all* relevant Φ values can be sampled in one run. We have not attempted to do so. Rather, we have performed a number of umbrella sampling in (partially overlapping) Φ 'windows.' The reason for doing so is the following. Let us assume that we sample an interval $\Phi_{max} - \Phi_{min} \equiv \Delta\Phi$ in n umbrella-sampling simulations. The optimum choice of n is clearly the one that samples the complete Φ interval in the minimum computing time. In order to estimate this time, let us assume that the system performs a random walk in Φ space within the window $\Delta\Phi/n$. Associated with the random walk in Φ space is a 'diffusion constant' D_Φ. The characteristic time needed to sample one interval $\Delta\Phi/n$ is

$$\tau_n = \frac{(\Delta\Phi/n)^2}{D_\Phi}.$$

Clearly, the total time to sample all n windows is

$$\tau_{tot} = n\tau_n = \frac{(\Delta\Phi)^2}{nD_\Phi}.$$

The important point to note is that the computing time *decreases* with increasing n. It would, however, be incorrect to assume that n should be chosen as large as possible. The actual equilibration time of a run in one of the Φ windows also depends on the rate at which all coordinates 'orthogonal' to Φ are sampled. Let us denote this time by $\tau_\perp$. Clearly, once $\tau_\perp$ becomes appreciably larger than τ_n, the total computation will scale as $n \times \tau_\perp$. This suggests that the optimum choice of n is the one for which $\tau_n \approx \tau_\perp$.

In our simulations, we used the results of a simulation of the first window to estimate w for the next (partially overlapping) window, and so on. Actually, for our purpose it is not essential that consecutive windows actually overlap. We wish to determine the variation of $F(\Phi)$ with Φ [see Eq. (1)]. If both $F(\Phi)$ and its derivative are smoothly varying functions of Φ, we can proceed as follows. We measure

$$\frac{\partial F(\Phi)}{\partial \Phi} = -k_B T \frac{\partial \ln P(\Phi)}{\partial \Phi}$$

in a finite number of (nonoverlapping) windows. We then fit

an analytic function (e.g., a polynomial in Φ) to these values of the free-energy derivative. Once we have an analytic expression for $[\partial F(\Phi)/\partial\Phi]$, we can integrate it to compute, for example, the height of the free-energy barrier. Although this version of umbrella sampling is not common, its molecular-dynamics equivalent is: In a 'constrained' MD simulation at fixed Φ, one measures the conjugate force $[\partial F(\Phi)/\partial\Phi]$ and uses this information to reconstruct $F(\Phi)$.

For simulations on small systems, there is no great advantage in the use of nonoverlapping windows. However, for large systems, it can be quite expensive to work with overlapping windows. In contrast, the nonoverlapping window approach will work equally well for small and for large systems.

III. ORDER PARAMETERS

In order to compute the free-energy barrier that separates the isotropic liquid from the crystalline state, we must first specify an order parameter that measures the degree of crystallinity in the system. It is important that this order parameter be chosen such that it does not favor one crystal structure over all others. This implies that our order parameter should be large for *all* crystalline phases and small for the isotropic fluid. Moreover, the value of the order parameter should be insensitive to the orientation of the crystal in space. And finally, it should be relatively easy to compute. As we shall see below, these requirements severely limit the number of useful order parameters.

A three-dimensional crystal is characterized by two distinct types of order that do not exist in an isotropic fluid, namely, translational order and orientational order. Translational order is commonly considered to be most characteristic feature of a crystal: The particle positions are repeated periodically in three independent directions. A quantitative measure of this translational order is the magnitude of the structure factor, $S(k)$, where the wave vector $\mathbf{k}$ is a basis vector (Bragg vector) in the reciprocal lattice corresponding to the crystal lattice under consideration. In simulations of a finite, periodic system, $\mathbf{k}$ should also be commensurate with the periodic boundary conditions of the system. It is easy to see that $S(\mathbf{k})$ does not satisfy the criteria for a 'good' order parameter that we have specified above. First of all, different lattices have different Bragg vectors. Hence, a choice of $\mathbf{k}$ that leads to a large value of $S(\mathbf{k})$ for one kind of lattice, may yield a small $S(\mathbf{k})$ for another lattice. In addition, the fact that $\mathbf{k}$ must be commensurate with the periodic box makes that a crystallite that is aligned with the periodic box, will appear to have a much larger degree of crystallinity than an identical crystallite that happens to be rotated with respect to the box edges.

There are, however, other measures of the order in a system that *are* rotationally invariant. For example, one can obtain detailed information about the local order in a many-body system by analyzing the Voronoi tessellation of space (see, e.g., Ref. 18). The Voronoi polyhedron associated with a given particle is defined as the set of points that are closer to that particle than to any other particle in the system. Clearly, the Voronoi polyhedra are convex and fill all space. One way to characterize a configuration of N atoms, is to count the number of triangular, square, pentagonal, etc. faces of the Voronoi polyhedron. It is customary to define the *signature* of a Voronoi polyhedron as a string of numbers that denote, successively, the number of triangular, square, pentagonal, etc. faces of the polyhedron. For example, the signature of a Voronoi polyhedron around a particle in a perfect bcc environment is (0608): its surface consists of 0 triangles, 6 squares, 0 pentagons, and 8 hexagons. In general, the instantaneous surroundings of a particle in a fluid or even solid will differ from those in a perfect crystal lattice. As a consequence, a given structure will be characterized by a *distribution* of Voronoi signatures, rather than a single one. Still, it is possible to use the Voronoi analysis to distinguish different crystal structures. However, the Voronoi signature does not provide a convenient *order parameter* to measure 'crystallinity.' The reason is that different crystal structures have very different Voronoi signatures, whereas, in the present study, we need an order parameter that is large for *all* crystal structures, while it should vanish (at least in the thermodynamic limit) for a disordered phase.

Another, rotationally invariant, measure of the crystallinity of a $3D$ system is provided by the *bond order* of the system. Orientational order, or bond order, is always present in three-dimensional crystals: The positional ordering of the particles implies that any particle is surrounded by other particles in certain preferred directions. As we shall see below, there exist quantitative measures of this bond order that are large for all crystal structures of interest and that are, moreover, invariant under rotation of the crystallite. For this reason, we shall use the degree of bond order in the system under study to quantify the degree of crystallinity in our simulations. As we shall show below, bond order is reasonably easy to calculate, and permits a neat differentiation to be made between isotropic and ordered states.

The bond-order parameters that we have used were introduced by Steinhardt *et al.*[38] and have been used by other authors to analyze the structure of a nucleating system.[20,14] The analysis starts with a definition of the neighbors of a particle (for instance, using the Voronoi construction). The vectors $\mathbf{r}$ joining neighbors are called bonds. Associated with every bond is a set of numbers

$$Q_{lm}(\mathbf{r}) \equiv Y_{lm}(\theta(\mathbf{r}),\phi(\mathbf{r})), \tag{6}$$

where $Y_{lm}(\theta,\phi)$ are spherical harmonics and $\theta(\mathbf{r})$ and $\phi(\mathbf{r})$ are the polar and azimuthal angles of vector $\mathbf{r}$ with respect to an arbitrary reference frame. Only even-l spherical harmonics are considered, because the permutation of a pair of (identical) particles ought not affect the bond-order parameter. The $Q_{lm}(\mathbf{r})$ defined in Eq. (6) are still *local* order parameters. We now define a global orientational order parameter $\overline{Q}_{lm}$ as

$$\overline{Q}_{lm} \equiv \frac{1}{N_b} \sum Q_{lm}(\mathbf{r}), \tag{7}$$

where the sum runs over all N_b bonds in the system. These $\overline{Q}_{lm}$ still depend on the choice of reference frame. However, from the $\overline{Q}_{lm}$, rotationally invariant combinations can be constructed:

$$Q_l \equiv \left(\frac{4\pi}{2l+1} \sum_{m=-l}^{l} |\overline{Q}_{lm}|^2 \right)^{1/2} \tag{8}$$

and

$$W_l \equiv \sum_{\substack{m_1,m_2,m_3 \\ m_1+m_2+m_3=0}} \begin{pmatrix} l & l & l \\ m_1 & m_2 & m_3 \end{pmatrix} \cdot \overline{Q}_{lm_1} \overline{Q}_{lm_2} \overline{Q}_{lm_3}. \tag{9}$$

Q_l and W_l are called second-order and third-order invariants, respectively. The term in brackets in Eq. (9) is a Wigner-3j symbol (see, e.g., Ref. 39). The order parameters Q_l and W_l still depend on the definition of neighbors that is used. In general, this is not a particularly serious problem. In any event, it is possible to define a reduced order parameter $\hat{W}$ that is hardly sensitive to the precise definition of the nearest neighbors of a particle:

$$\hat{W}_l \equiv W_l \Big/ \left(\sum_m |Q_{lm}|^2 \right)^{3/2}. \tag{10}$$

These $\hat{W}_l$ provide a convenient quantitative measure for the prevalent crystal structure of the system under study. In Table I, some low-l order parameters are given for simple cluster geometries. Of these only the icosahedral geometry cannot be repeated periodically to fill all space. For symmetry reasons the first nonzero values occur for $l=4$ in clusters with cubic symmetry and for $l=6$ in clusters with icosahedral symmetry. Inspection of Table I shows that knowledge of all four order parameters listed allows us to distinguish the most common structural units of simple atomic systems. All order parameters listed in Table I vanish in the isotropic fluid phase, at least in the thermodynamic limit. As can be seen from Table I, the order parameter Q_6 is of the same order of magnitude for *all* crystal structures of interest. This makes Q_6 less useful to distinguish different crystal structures, but very useful to act as a generic measure of crystallinity. For this reason, we have selected Q_6 to play the rôle of *the* crystalline order parameter in all our simulations. The 'reaction coordinate' from isotropic liquid to crystal therefore corresponds to a path of increasing Q_6. The other order parameters that were discussed in the present section have been used to analyze the nature of the crystalline structures formed in our simulations.

IV. COMPUTER SIMULATIONS

A. Introduction

As an illustration of the techniques described in the previous sections, we have performed a series of computer simulations to measure the variation of the free energy of a simple atomic system with the 'crystallinity' order parameter Q_6. We selected a model about which much is known from other simulations, namely, a system of particles interacting through an r^{-12}-soft-sphere potential,

$$v(r) = \epsilon(\sigma/r)^{12}. \tag{11}$$

The model parameters ϵ and σ can be used to construct dimensionless expressions for the density ($\rho^* \equiv \rho\sigma^3$), the temperature ($T^* \equiv k_B T/\epsilon$) and the pressure ($P^* \equiv P\sigma^3/\epsilon$). In fact, the thermodynamic state of this model system can be completely specified by a single dimensionless parameter, namely, the reduced density

$$\rho' \equiv \frac{N\sigma^3}{V} (\epsilon/k_B T)^{1/4} = \rho^* (T^*)^{-1/4}. \tag{12}$$

However, in order to facilitate comparison with other model systems we prefer to specify T^* and P^* separately.

In view of the exploratory nature of the present work, most calculations were performed on quite small periodic systems containing 125 or 128 particles. The former system size is a 'magic number' for a bcc crystal, while the latter number is optimal for an fcc crystal. We cannot hope to extract quantitative estimates on nucleation barriers from simulations of such small systems. However, as simulations of such small systems are relatively cheap, we can easily study a number of different supercoolings and different initial conditions. This allows us to discuss most of the practical aspects of the simulation technique. In our simulations of these small systems, we found that the free-energy barrier separating the fluid from the (stable) fcc phase was, invariably, much higher than the barrier between the fluid and a bcc crystal. In order to test whether this trend is an artifact of the small system size, we performed one simulation for a larger system ($N=1000$) at 20% supercooling. This simulation confirmed that it is relatively easy to go from the fluid to the bcc phase, yet it also showed that the *magnitude* of the free-energy barrier is quite sensitive to the system size. However, the simulation of the 1000-particle system also demonstrates that the techniques that we employ are not limited to small systems. Hence, the fact that relatively large systems must be studied in order to arrive at a quantitative estimate of the nucleation barrier does not constitute a serious problem.

TABLE I. Bond orientational order parameters [see Eqs. (8) and (10)] for a number of simple cluster geometries. fcc: face-centered-cubic structure, hcp: hexagonal close-packed structure, bcc: body-centered-cubic structure, and sc: simple cubic structure.

Geometry	Q_4	Q_6	$\hat{W}_4$	$\hat{W}_6$
Icosahedral	0	0.663 32	0	−0.169 754
fcc	0.190 94	0.574 52	−0.159 317	0.013 161
hcp	0.097 22	0.484 76	0.134 097	−0.012 442
bcc	0.036 37	0.510 69	0.159 317	0.013 161
sc	0.763 76	0.353 55	0.159 317	0.013 161
(liquid)	0	0	0	0

B. Computational details

All simulations were carried out at constant pressure, using the Monte Carlo scheme described in Ref. 40. The reason to carry out simulations at constant pressure, rather than at constant volume is that former condition corresponds more closely to the experimental situation. This is of particular importance near coexistence. Using a constant pressure simulation it is possible, at least in principle, to transform one phase, at constant temperature and pressure, into the other phase with which it coexists. This is not possible in constant NVT simulations. If we measure the distribution function $P(Q_6)$ at constant pressure, rather than at constant volume, we obtain information about the Gibbs free-energy barrier between the solid and the liquid phase. Eq. (1) is consequently replaced by

$$G(Q_6) = -kT \ln P(Q_6), \tag{13}$$

where we have included the constant term in $G(Q_6)$. In our simulations, we have used truncated octahedral periodic boundary conditions.[41] The choice of such an almost spherical box shape should minimize the effect of the periodic boundary conditions on the preferred crystal structure of the system. The r^{-12}-soft-sphere potential was truncated at a distance $r_c^* \equiv r_c/\sigma$. The long-range contribution to the potential was computed under the assumption that the density is constant for $r^* > r_c^*$. For r^{-n}-soft spheres, the potential energy scales with volume as $\mathscr{V} \sim V^{-n/3}$. This property makes it easy to perform volume changes in a constant *NPT* simulation of such a system, provided that all cutoff radii are scaled with the linear dimensions of the simulation box. In our simulations, the cutoff distance for the intermolecular interactions was chosen such that $r_c^* = 2.0$ at a density $\rho^* = 1.217$, which corresponds to the density of an fcc crystal at coexistence [$P^* = 24.21$, $T^* = 1.0$ (Ref. 42)].

As discussed in Sec. III, we measure bond-orientational order parameters to monitor the crystallinity of the system. In order to evaluate these order parameters, we must specify the nearest neighbor of a particle. The precise numerical values obtained for Q_l will depend somewhat on the definition of nearest neighbors (the $\hat{W}_l$ are expected to be less sensitive). However, any reasonable definition of nearest neighbors will lead to the same qualitative behavior.[38] Hence, it is reasonable to choose the definition that is computationally most convenient.[38] In our simulations, we used the following 'recipe': all particles within a certain cutoff radius r_q^* from a given particle were considered to be its neighbors. The cutoff distance was chosen to be $r_q^* = 1.30$, which corresponds to the first minimum of $g(r)$ in an fcc crystal at coexistence. A neighbor list (see, e.g., Ref. 43) with a range $r_N^* = 2.5$ was used to speed up the calculation.

Each MC step consisted either of a trial displacement of a particle or a trial volume change. The choice between trial displacements and volume changes was made at random, with 8% probability for the latter. We tried to maintain the acceptance ratio of MC trial moves at approximately 50%. A simulation started with an equilibration period of 1000–1500 cycles followed by a production run of 10 000–15 00 cycles (during one cycle we perform, on average, one test displacement per particle).

All simulations were started either from a crystalline state or from a liquid configuration, obtained by melting a crystal at low pressure. The first run in a series of umbrella samplings was performed without any weight function. The resulting $G(Q_6)$ was extrapolated by fitting to a polynomial in Q_6

$$G'(Q_6) = a_0 + a_1 Q_6 + a_2 Q_6^2 + \cdots. \tag{14}$$

A successive simulation was then performed on an interval in Q_6 bordering the range of Q_6 spanned by the previous run, with a weight function $w(Q_6) = \exp[\beta G'(Q_6)]$. Every individual simulation yields only part of the (as yet, unnormalized) distribution function $P(Q_6)$. In order to construct a single, normalized probability distribution function, a simultaneous polynomial fit of the function $\ln P(Q_6)$ in consecutive windows was performed to construct a single function that varied smoothly as a function of Q_6. In these fits, the coefficients Q_6, Q_6^2,... were kept the same for a pair of neighboring windows, while the constant term was adjusted to provide a smooth match. Once $P(Q_6)$ in all consecutive windows has thus been connected, we are left with a single, normalized distribution function from which we can derive the free-energy barrier with help of Eq. (13).

Most of the techniques to analyze the structural properties of the system have already been discussed above. We only should add that Voronoi tessellation of space was calculated using a standard algorithm,[43] while the structure factors were calculated by fast Fourier transform of the particle densities along the three principal axes of the simulation box.[44]

V. RESULTS AND DISCUSSION

As discussed in Sec. I, previous molecular dynamics simulations of homogeneous nucleation could only be performed in strongly supercooled (or overcompressed) systems. In contrast, the present approach makes it possible, at least in principle, to study the free-energy barrier between two phases at an arbitrary temperature. We therefore started our study at the coexistence temperature, precisely because this represents a *worst case* for conventional nucleation studies. We stress, however, that the free-energy barrier between solid and liquid at (or close to) coexistence is completely dominated by finite-size effects and is not related to the free-energy barrier for homogeneous nucleation in a bulk fluid. In fact, in the thermodynamic limit, homogeneous nucleation at the coexistence temperature is impossible, since the critical nucleus would be infinitely large. But in a finite, periodic system, the free-energy barrier between solid and liquid is finite. It corresponds to the reversible work needed to create the interface between the coexisting liquid and solid. A macroscopic estimate suggests that this barrier should be of the order $\Delta G = 2\gamma_{\text{solid-liquid}} L^2$, where $\gamma_{\text{solid-liquid}}$ is the surface free-energy density of the solid–liquid interface, while L denotes the diameter of the simulation box. It should, however, be pointed out that the surface free energy γ_{SL} in a finite, periodic system will, in general, differ from this 'macroscopic' estimate if the system size is not much larger than the interface thickness.[45] Clearly, such finite-size effects are most serious in the vicinity of a critical point, where this width diverges. But, even though the present simulations were not performed near a critical point, we should expect finite-size effects to be important in a 3*D* system with $\mathscr{O}(10^2)$ particles. Hence, the height that we compute for the free-energy barrier between the coexisting solid and fluid will not provide a reliable estimate of the bulk solid–liquid surface free energy. Anyway, as it was not our purpose to compute the latter quantity, we have not attempted to measure the height of the solid–liquid free-energy barrier in larger systems, although this is certainly feasible.

Subsequently, we discuss simulations of the free-energy barrier between the solid and a *supercooled* liquid. In this case, the height of the free-energy barrier in the thermodynamic limit corresponds to the barrier to homogeneous crystal nucleation. Again, finite-size effects can be important: both the width of the solid–fluid interface and the size of the

TABLE II. Literature data on the location of the solid–liquid coexistence point of r^{-12}-soft spheres.

P^*	ρ^*_{liquid}	ρ^*_{crystal}	Ref.
22.56 ± 0.4	1.150	1.194	46
24.21	1.173	1.217	42

critical nucleus itself should be much smaller than the diameter of the simulation box. Again, we do not expect this condition to be fullfilled for systems of $\mathcal{O}(10^2)$ particles. We have therefore included one simulation on a much larger system (10^3 particles) in order to show that the qualitative trends that we observe in small systems is not an artefact of the small system size.

A. Simulations at coexistence

Table II contains the available data about the melting point of r^{-12}-soft spheres. We have used the more recent data of Ogura *et al.*[42] to estimate the location of the melting point.

We first studied a system consisting of 128 particles, starting both from a perfect fcc crystal and from a well-equilibrated fluid. The results of these simulations are discussed most easily with the help of Fig. 1. In this figure, the free energy is plotted as a function of Q_6. Three separate branches are visible, each corresponding to the results of several individual simulations. When Q_6 is lowered, starting from the fcc crystal, the free energy increases by 18 $k_B T$, after which the crystal suddenly melts to the liquid state. As the transition from solid to liquid occurs irreversibly, we cannot construct a single free-energy curve from these simulations. However, as Ref. 42 indicates that the fcc solid should coexist with the liquid at this temperature and pressure, we have drawn Fig. 1 such that $P(Q_6)$ in the liquid state is normalized to the same value as $P(Q_6)$ in the fcc solid. In other words, the Gibbs free energy of the liquid state and the fcc crystal are equal. We shall come back to this point later.

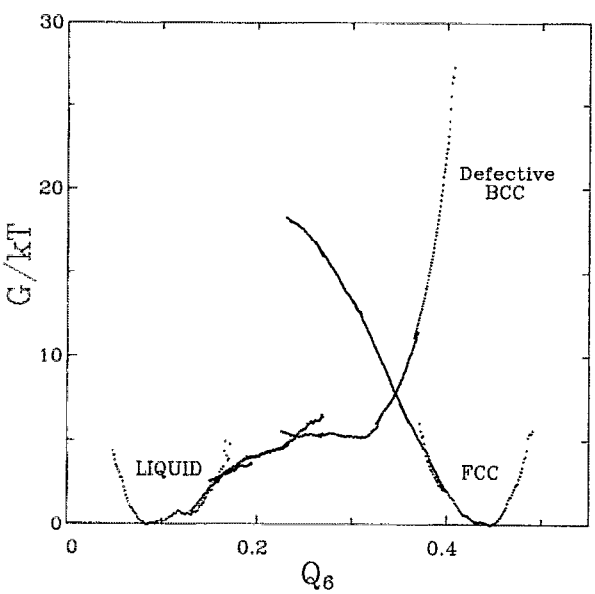

FIG. 1. Gibbs free energy near coexistence ($P^* = 24.21$ and $T^* = 1$) for a 128-particle r^{-12} system as a function of Q_6. The three different branches correspond to the liquid, the defect-rich bcc crystal that has formed from the liquid and the fcc crystal. In drawing this figure, we have assumed that the liquid and fcc phases are in equilibrium (Ref. 42) and therefore have the same Gibbs free energy. The Gibbs free energy of the defect-rich bcc state is estimated in the way indicated in the text.

Next consider what happens if we start our series of simulations from the liquid side. In this case we find that, as Q_6 is increased, the Gibbs free energy rises slightly (some $5k_B T$), and then goes down again. Subsequent analysis, including visual inspection of the atomic configurations, revealed that a bcc-like structure (with some defects) had formed. The occurrence of such defects is not surprising as the simulation box cannot accommodate a perfect bcc crystal with 128 particles.

From Fig. 1 it is clear that the weighted sampling scheme permits the free energy $G(Q_6)$ to be determined in a regime that is never probed in an unbiased sampling scheme. Clearly, the present approach in which only one order parameter is used as a control variable does not constrain the system to move along a single trajectory in configuration space: Some hysteresis does occur and the system can suddenly jump to another state. This fact creates a problem, because we can only compute free-energy differences between states that are connected by a reversible path. However, we can bracket the relative Gibbs free energy of the fluid and bcc-like branches by observing that the hysteresis between them is quite small. Using the fact that the irreversible transition from one branch to another can only occur if this results in a lowering of the Gibbs free energy of the system, we can estimate the relative Gibbs free energy of the liquid and bcc branches to within 1 $k_B T$. This is surprisingly accurate, if one bears in mind that 1 $k_B T$ is the error in the *total* Gibbs free energy. The error in the Gibbs free energy per particle is of the order 0.01 $k_B T$. Such an accuracy is only marginally worse than what is obtained with 'standard' free-energy calculations for the solid–liquid transition.

The formation of bcc crystals from the liquid will be examined in some detail below. First, however, we discuss the behavior of the order parameters during the simulations. Figure 2 shows a correlation plot of the parameters Q_4, $\hat{W}_4$, and $\hat{W}_6$ as a function of Q_6.

During the simulations the values of these parameters were calculated at regular intervals (for example, every ten cycles). Each one of these measurements corresponds to a dot in the figure. The vertical streaks in the figure are caused by the fact that several simulations, each for another interval of Q_6, are combined in one plot. For comparison, the values for perfect clusters are shown in the same figure. In addition, we have computed the equilibrium values of all order parameters in the fcc, bcc, and liquid state, at the same temperature and pressure. These are indicated in the figure by single, boldface letters (**F**, **B**, and **L**, respectively). The fact that the order parameters are nonzero in the liquid state is a finite-size effect. Note that these finite-size effects are much larger in Q_4 and Q_6 which are, by construction, positive than in the $\hat{W}_l$. What is particularly noteworthy in Fig. 2 is that the

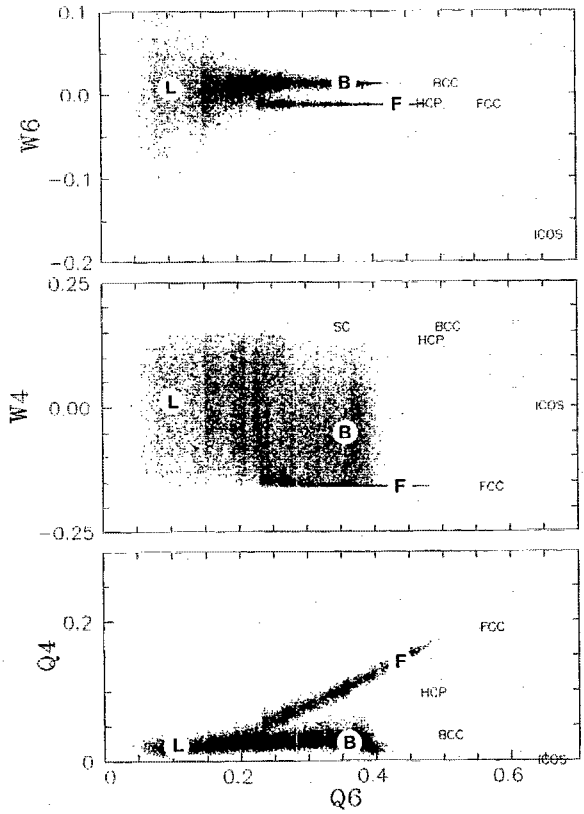

FIG. 2. Correlation plot for order parameters Q_4, W_4, and W_6 as a function of Q_6, for the r^{-12} system near coexistence ($P^* = 24.21$ and $T^* = 1$). The number of particles in the system is either 125 or 128. The values for perfect cluster geometries listed in Table I are indicated by their abbreviations. The letters L, F, and B refer to the equilibrium averages for the liquid phase, the fcc crystal and the bcc crystal, respectively.

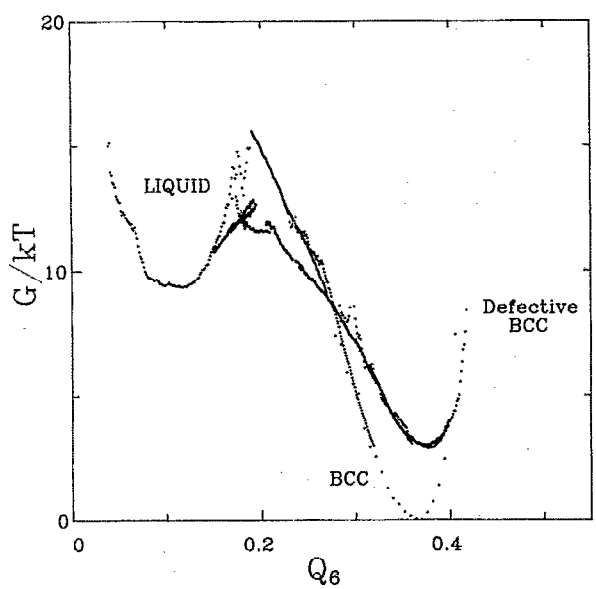

FIG. 3. Gibbs free energy as a function of Q_6 for the r^{-12} system with 125 particles near coexistence ($P^* = 24.21$ and $T^* = 1$). The three different branches correspond to the liquid, the strained bcc crystal formed from the liquid and the bcc crystal. The offsets for the liquid and the strained bcc state with respect to the bcc crystal are estimated as indicated in the text.

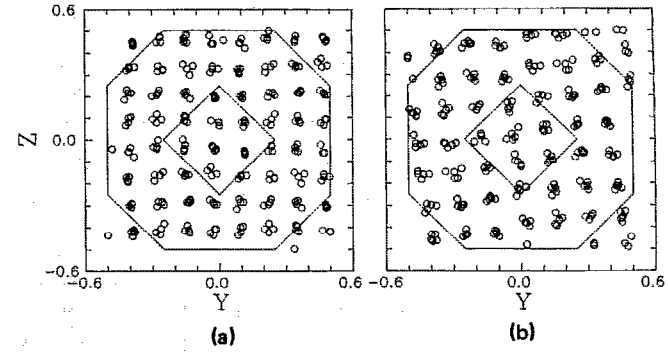

FIG. 4. Snapshots of the atomic coordinates in two crystalline phases of an r^{-12} fluid near coexistence ($P^* = 24.21$ and $T^* = 1$). For the sake of clarity we have drawn all periodic images of particles that lie within the cube enclosing the truncated octahedral simulation box. The contours of the simulation box are indicated in the figure. (a) fcc crystal with 128 particles and (b) strained bcc crystal with 125 particles, prepared by increasing the crystallinity (Q_6) of the liquid.

order parameter distributions for the fcc state are clearly different from those of the liquid and the bcc phase. The latter two can, in fact, not be distinguished in this figure and none of the order-parameter distributions plotted in this figure shows any hint of a sharp transition between these two states. Apparently the bond-order fluctuations in the liquid are rather bcc-like and very different from the corresponding fluctuations in the fcc phase. Evidence for bcc-like ordering in the liquid state has also been reported by Robbins *et al.*[21] for the Yukawa fluid.

Another point to note is that the second-order invariants Q_4 and Q_6 are considerably smaller in the 'warm' equilibrium crystal than in the perfect clusters. For the reduced invariants $\hat{W}_l$ this effect is expected to be weaker. For $\hat{W}_6$ this is indeed found to be the case. However, $\hat{W}_4$ in the bcc phase is found to fluctuate wildly (as wildly, in fact, as in the liquid state) and $\langle \hat{W}_4 \rangle$ bears no resemblance to the value found for the ideal cluster. This indicates that $\langle \hat{W}_4 \rangle$ is not a convenient measure of bcc-like order. In order to investigate the transformation between fluid and bcc crystal more carefully, we repeated the above calculations with 125 particles. The corresponding free energy curves are shown in Fig. 3. The perfect bcc crystal behaves much like the perfect fcc crystal before. It melts after climbing a free-energy barrier of about $16k_BT$. Starting from the liquid, a barrier of about $4k_BT$ was found to separate the liquid from a imperfect bcc state that, again, formed spontaneously as Q_6 was increased. However, this time, the crystal that formed contained far fewer defects than the one formed in the 128-particle system. In fact, the particles were found to be located in regular lattice positions, but the lattice as a whole was rotated with respect to the simulation box (see Fig. 4). Other authors have observed very similar rotated crystallites in numerical studies of crystal nucleation.[22]

Figure 5 shows $S(\mathbf{k}_{max})$ as a function of $\langle Q_6 \rangle$. The $\mathbf{k}_{max}$ correspond to the maxima of $S(\mathbf{k})$ along the x, y, and z directions. As expected, $S(\mathbf{k}_{max})$ is large in the ordered crystals

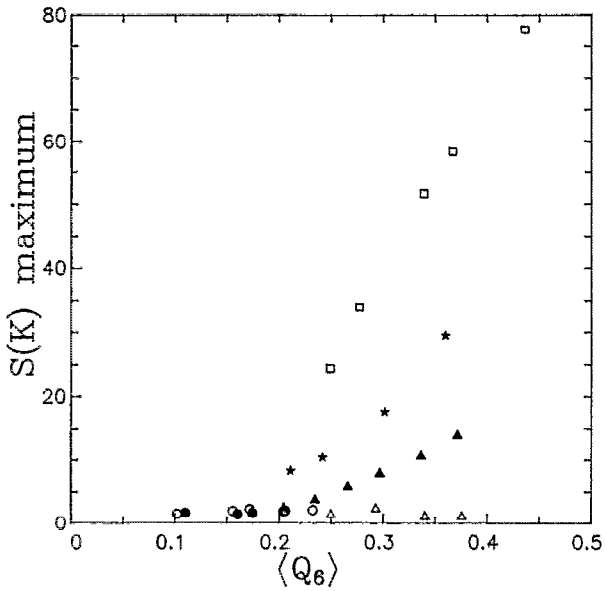

FIG. 5. Maximum value of the structure factor $S(\mathbf{k})$, averaged along the three edges of the simulation box, as a function of the average Q_6. The liquid is indicated with circles, the fcc crystal with squares, the bcc crystal with stars, and the imperfect bcc crystal with triangles. Open symbols: $N = 128$, filled symbols: $N = 125$.

but small in the liquid phase. However, this figure also shows why $S(\mathbf{k}_{\max})$ is *not* a good generic order parameter for crystallinity: the maximum of $S(\mathbf{k})$ for the imperfect bcc phase of the 128-particle system is even lower than that of the liquid. In other words, the maximum value of the structure factor is strongly affected by the presence of crystal defects and by the rotation of the crystallite. Note also that $S(\mathbf{k}_{\max})$ is still liquidlike at the Q_6 value that corresponds to the maximum in the free-energy barrier between the liquid and the bcc phase.

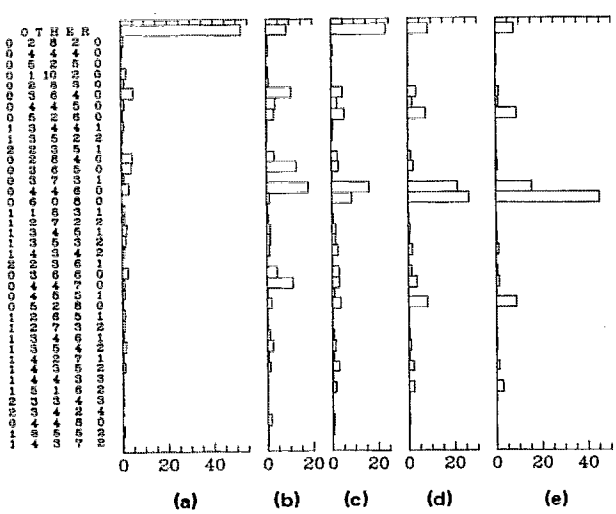

FIG. 6. Histograms of the most prevalent Voronoi signatures for the r^{-12} system near coexistence. The relative abundance of the most important signatures is indicated in the figure. $N = 128$ (a) liquid, (b) fcc crystal, and (c) defect-rich bcc crystal formed from the fluid. $N = 125$ (d) bcc crystal and (e) bcc crystal formed from the fluid. These histograms are based on averages over 10–30 atomic configurations that were analyzed during the simulations.

The results of the Voronoi analysis are given in Fig. 6. The liquid state shows a broad distribution of different signatures. The fcc crystal has a pronounced (0446) signature but, unlike the bcc phase, it has no (0608) signature. The Voronoi signature of the 128-particle defect-rich bcc phase is very similar to that of the perfect crystal. This is a good indication that the structure really is bcc-like. Somewhat surprisingly, the 125-particle strained bcc phase shows a stronger (0608) signal. We shall come back to this point later.

One feature of Fig. 3 is rather unexpected, namely, that the bcc phase appears to have a lower Gibbs free energy than the liquid state. As the simulations were performed at the melting temperature and pressure estimated by Ogura *et al.*,[42] we would expect the liquid to have the same Gibbs free energy as the fcc phase. According to the work of Hoover *et al.*,[7] the bcc phase should then be less stable than the fcc phase. Hence, we would have expected to find that the bcc phase would have a *higher* Gibbs free energy than the fluid. However, as Fig. 3 shows, the Gibbs free energy of the imperfect bcc state (which can be reached from the fluid without much hysteresis) is some 7 $k_B T$ lower than that of the liquid. According to Ref. 7, the Gibbs free energy of the fcc state should be still lower. This suggests that the pressure at which we have performed our simulations is, in fact, higher than the coexistence pressure for this system. As mentioned above, we used the coexistence pressure reported by Ogura *et al.*[42] (see Table II). This pressure is higher than the one reported by Hoover[46] ($\Delta P^* = 1.7$). Using the Gibbs–Duhem relation, we can estimate how much the Gibbs free-energy difference between solid and liquid would change if we lowered the pressure to the value proposed by Hoover. Using

$$\left(\frac{\partial \Delta G^*}{\partial P^*}\right) = N\Delta\left(\frac{1}{\rho^*}\right) \tag{15}$$

and the solid and liquid densities given in Table II we find that $\Delta(\Delta G^*) \approx 3.9 \Delta P^*$. If we insert $\Delta P^* = 1.7$, we obtain $\Delta(\Delta G^*) \approx 6.7$. This accounts for a large fraction of the Gibbs free-energy difference between the solid and the liquid phase shown in Fig. 3. In any case, there is no reason to expect coexistence in a finite system to be located at exactly the same pressure as in the infinite system.

B. Simulations in supercooled systems

In this section we describe the results of simulations in which we measured the free-energy barrier to crystal formation at finite supercooling. In our calculations, we chose to use moderate supercoolings, $T^* = 0.8$ and $T^* = 0.6$, respectively (the pressure was maintained at $P^* = 24.21$). It should be stressed that this degree of supercooling is less than what is typically imposed during molecular-dynamics studies of homogeneous nucleation. First, we performed simulations on small systems ($N = 125$ and $N = 128$) at $T^* = 0.8$ and $T^* = 0.6$. Next, we repeated the simulations at $T^* = 0.8$ with a much larger system ($N = 1000$), in order to test for finite-size effects. In all the simulations reported be-

low we find that a bcc phase forms as the 'crystallinity' of the fluid phase is increased. For the small systems, this observation did not depend on whether the number of particles corresponds to a 'magic number' for a perfect fcc or bcc lattice ($N = 128$ and $N = 125$, respectively). In what follows, we therefore do not describe the simulations of the 128-particle system, as these provided the same information as obtained in simulations of the 125-particle system.

C. 125-particle system

The (Gibbs) free-energy curves of the 125-particle system at $T^* = 0.8$ are shown in Fig. 7. The crystalline structure that is formed from the fluid phase is characterized by values of the various order parameters and by a Voronoi histogram that are typical of a (defect-rich) bcc phase. However, inspection of the atomic coordinates of this structure (see Fig. 8) shows that the particles are certainly not arranged on the lattice positions of a well-aligned bcc crystal. As can be seen from Fig. 7, the resulting structure has a Gibbs free energy that is about $10k_BT$ higher than that of the perfect bcc crystal. The most important thing to note in Fig. 7 is that there is, in fact, no trace of a free-energy barrier for the formation of a bcc crystallite! Our simulations indicate that, even at this moderate degree of supercooling, the isotropic liquid phase is absolutely unstable. The same observation applies, *a fortiori* to the system at a reduced temperature $T^* = 0.6$ (see Fig. 9). In this case, the structure that happened to form from the liquid phase was rather similar to that observed at $T^* = 1.0$: All particles were regularly placed in a distorted bcc structure that was rotated with respect to the simulation box (see Fig. 8). As the liquid phase at $T^* = 0.6$ and $T^* = 0.8$ is not even metastable, we can only make a rough estimate of the Gibbs free-energy difference between the fluid and the bcc solid. For $T^* = 0.8$ we estimate that the Gibbs free-energy difference between liquid and bcc crystal is about $30k_BT$ (i.e., $0.24k_BT$ per particle), while for $T^* = 0.6$, this difference amounts to approximately $60k_BT$ ($0.48\ k_BT$ per particle). Our simulations of a 1000-particle system (see below) show that, at least at $T^* = 0.8$, the complete disappearance of a free-energy barrier between the supercooled fluid and the bcc phase is a finite-size effect. However, also for the larger system, we find that the free-energy barrier between liquid and bcc crystal is quite low.

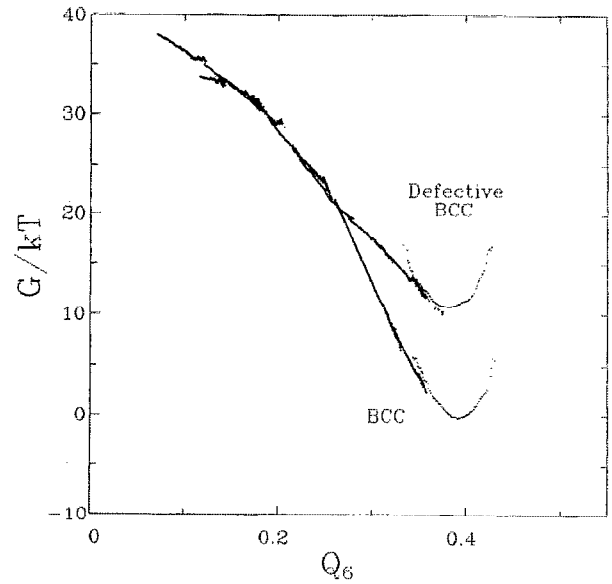

FIG. 7. Free energy as a function of Q_6 for 125 r^{-12} particles at $T^* = 0.8$ and $P^* = 24.21$.

Figure 10 shows the order-parameter distributions for the phase that formed from the fluid at $T^* = 0.6$. Comparison of this figure with the corresponding plots in Fig. 2 confirms the bcc nature of the crystalline phase that has formed.

The Voronoi analysis of the ordered and imperfect crystalline structures at $T^* = 0.8$ and $T^* = 0.6$ are shown in Fig. 11. What is remarkable is that the ordered bcc crystal, although dominated by the (0608) signature, shows many other signatures as well, while the strained structures show a very strong (0608) signal. The same trend is already apparent at $T^* = 1.0$ (Fig. 6).

Table III contains a summary of the average density and bond-order parameter for all liquid, crystalline, and 'nuclea-

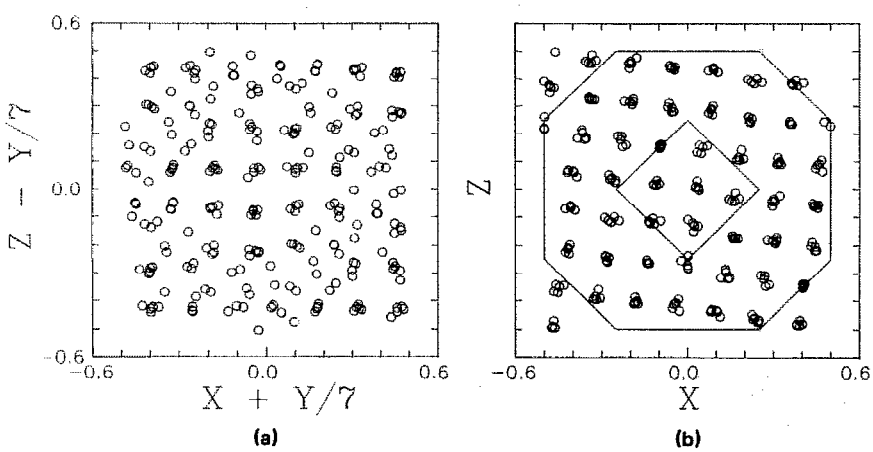

FIG. 8. Snapshots of the atomic configuration in a 125-particle r^{-12} system at $P^* = 24.21$. For the sake of clarity we have drawn all periodic images of particles that lie within the cube enclosing the truncated octahedral simulation box. The structures that are shown were formed from the liquid by increasing Q_6. (a) $T^* = 0.8$. Projection on the plane $x - 7y - z = 0$. (b) $T^* = 0.6$. Projection on the plane $y = 0$. The contours of the simulation box are indicated in the figure.

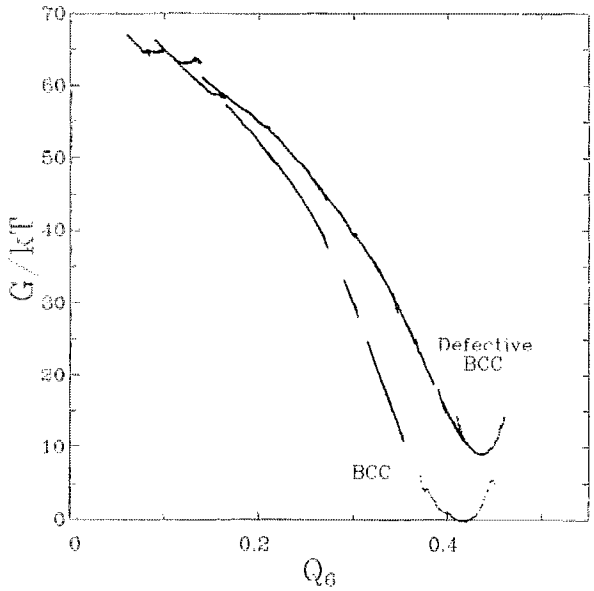

FIG. 9. Gibbs free energy of a 125-particle r^{-12} system as a function of Q_6 at $T^* = 0.6$ and $P^* = 24.21$.

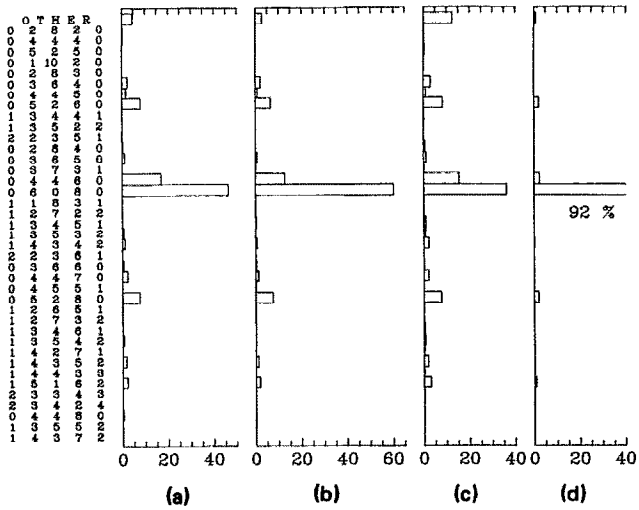

FIG. 11. Histograms of the most prevalent Voronoi signatures for the r^{-12} system at $P^* = 24.12$ and $T^* = 0.6$ and 0.8. The relative abundance of the most important signatures is indicated in the figure. These histograms are based on averages over 10 atomic configurations that were analyzed during the simulations. (a) bcc crystal at $T^* = 0.8$ and (b) bcc crystal at $T^* = 0.6$; (c) defect-rich bcc state at $T^* = 0.8$, and (d) strained bcc state at $T^* = 0.6$.

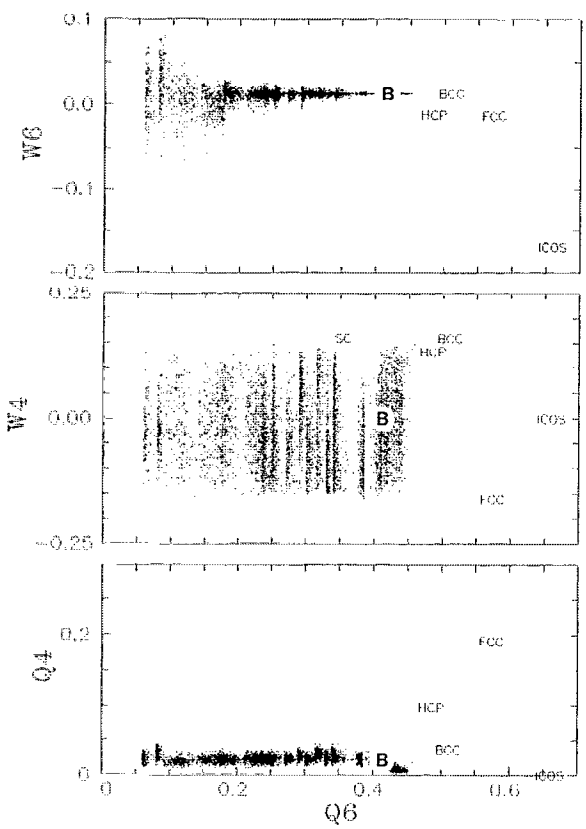

FIG. 10. Correlation plot for the order parameters Q_4, W_4, and W_6 as a function of Q_6, for a 125-particle r^{-12} system at $T^* = 0.6$ and $P^* = 24.21$. The values for the perfect cluster geometries listed in Table I are indicated by the corresponding abbreviations. The letter B refers to the equilibrium average for the bcc crystal.

ted' phases that we have studied. The table clearly shows how both ρ^* and $\langle Q_6 \rangle$ increase with decreasing temperature. When we compare the bcc crystallites formed from the liquid with the corresponding perfect crystal structures, we find that the latter has a slightly higher density. However, $\langle Q_6 \rangle$ is, if anything, lower for the ordered crystal than for the phase that formed from the fluid. As with the Voronoi signatures, the strained, imperfect state appears to have more local order than the perfect crystalline state. At this stage we have no simple explanation for this observation.

D. 1000-particle system

We performed two sets of simulations of a 1000-particle system at $T^* = 0.8$: In the first, the system was prepared in the fluid phase. Subsequently, the crystallinity was slowly increased. The curves Fig. 12 have been constructed using data of umbrella-sampling simulations in a number of adjacent Q_6 windows. Note, however, that there are a several gaps in these sets of data points. Nevertheless, we can construct the desired free-energy curves, even though we have not collected statistics on $P(Q_6)$ over the entire Q_6 range of interest. This illustrates the remarks about umbrella sampling of large systems, made at the end of Sec. II. In contrast to what is observed in the 125-particle system, we find that the Gibbs free energy increases initially. It goes through a maximum at a value of $Q_6 \approx 0.13$ and then goes down again (see Fig. 12). The height of the free-energy barrier is quite small ($G/k_B T \approx 25$). As before, we find that the crystalline structure that forms from the isotropic liquid is an imperfect bcc phase. This is illustrated by Fig. 13 which shows the Voronoi signature of the crystal phase that is formed from the fluid by increasing the crystallinity. In the same figure, we also show the Voronoi signature of the fluid and of a

TABLE III. Average values ρ^* and $\langle Q_6 \rangle$ in the different metastable states at of the r^{-12} system at coexistence and at moderate supercooling. In all cases, the reduced pressure equals $P^* = 24.21$. These data were collected in normal (unbiased) Monte Carlo simulations. No data are given for the low-temperature liquid, as this phase was not even metastable (see text).

T^*	N		Liquid	'Nucleated' solid	bcc crystal	fcc crystal
1.0	125	$\langle \rho^* \rangle$	1.178	1.206	1.209	...
		$\langle Q_6 \rangle$	0.110	0.371	0.360	
	128	$\langle \rho^* \rangle$	1.177	1.190	...	1.217
		$\langle Q_6 \rangle$	0.102	0.273		0.436
0.8	125	$\langle \rho^* \rangle$	...	1.220	1.230	...
		$\langle Q_6 \rangle$		0.381	0.391	
	128	$\langle \rho^* \rangle$	...	1.216	...	...
		$\langle Q_6 \rangle$		0.335		
0.6	125	$\langle \rho^* \rangle$	...	1.247	1.249	...
		$\langle Q_6 \rangle$		0.435	0.414	
	128	$\langle \rho^* \rangle$	...	1.237	...	...
		$\langle Q_6 \rangle$		0.377		

system that was prepared and equilibrated in the bcc phase. We used the latter system as the initial configuration for a series of runs in which the crystallinity was *decreased*. As can be seen in Fig. 12, there is little evidence of hysteresis around the peak of the Gibbs free-energy barrier. This is encouraging, because it indicates that the nucleation barrier in a large system can, in fact, be computed with reasonable accuracy. Still, we should be careful in interpreting the barrier of $25k_BT$ as *the* barrier for homogeneous nucleation. At a supercooling of only 20%, we should expect to have quite a large critical nucleus. Hence, the condition that this nucleus is much smaller than the system size may not be satisfied. A nice feature of the present approach is that it allows us to make a snapshot of the critical nucleus. Figure 14 shows the atomic configuration of the 1000-particle system, at the top of the free-energy barrier. For the sake of clarity, the snapshot has been periodically repeated over several simulation boxes. It is important to note that the crystallinity is not distributed homogeneously over the system. In other words, the free-energy barrier that we measure is indeed associated with the formation of a localized crystal nucleus. However, as can be seen in Fig. 14, the size of the crystalline region is not small compared to the dimensions of the simulation box. Hence, we may expect to find some interaction between the periodic images of the critical nucleus. This could affect the apparent height of the nucleation barrier. In order to eliminate this effect, we would have to go to still larger systems or,

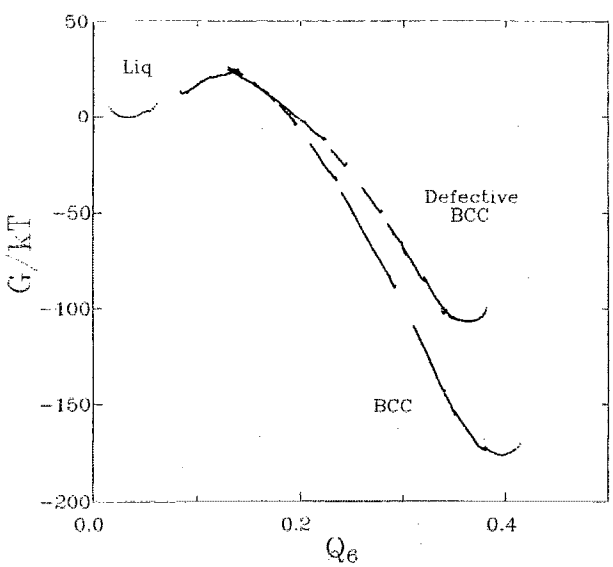

FIG. 12. Gibbs free energy of a 1000-particle r^{-12} system as a function of Q_6 at $T^* = 0.8$ and $P^* = 24.21$.

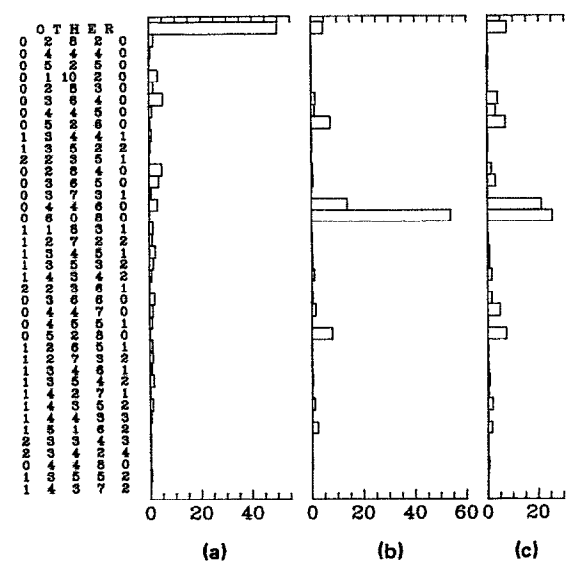

FIG. 13. Histograms of the most prevalent Voronoi signatures for a 1000-particle r^{-12} system at $P^* = 24.12$ and $T^* = 0.8$. The relative abundance of the most important signatures is indicated in the figure. (a): supercooled fluid, (b): bcc crystal, (c): imperfect bcc crystal formed from liquid. These histograms are based on averages over 10–20 atomic configurations that were stored during the simulations.

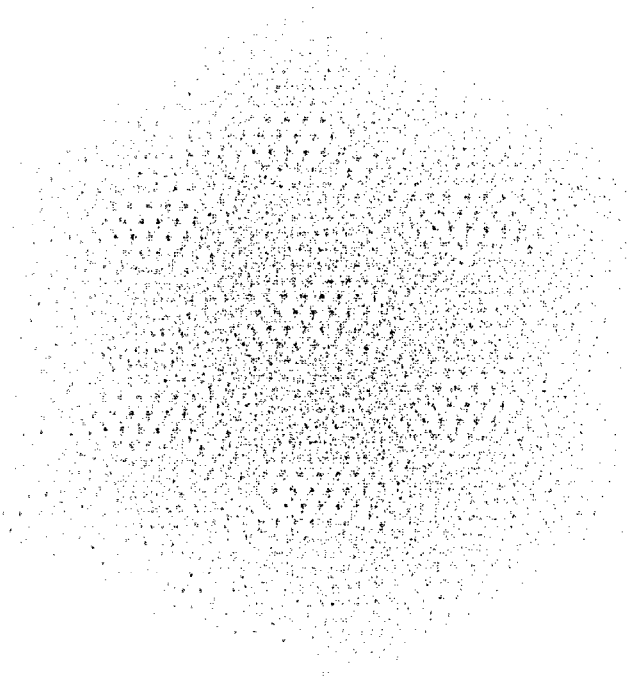

FIG. 14. Snapshot of the atomic configuration at the top of the Gibbs free-energy barrier in a 1000-particle r^{-12} system at $P^* = 24.21$ and $T^* = 0.8$. For the sake of clarity we have drawn 16 periodic images of the original simulation box. The crystallite that is shown was formed from the liquid by increasing Q_6.

alternatively, study the same system at larger supercooling where the critical nucleus is expected to be smaller. We have not attempted to study larger system sizes. Although such a study might yield a slightly different quantitative estimate of the nucleation barrier, we do not believe that it would affect our qualitative conclusion that for the r^{-12} system, the fluid at moderate supercooling is separated by a much lower Gibbs free-energy energy barrier from the metastable bcc solid than from the stable fcc solid.

VI. CONCLUSION

In this paper we have shown how Monte Carlo simulations can provide information about the height of the Gibbs free-energy barrier that separates the liquid and crystalline phase in an atomic system. In order to measure such a free-energy barrier, we had to select a convenient 'reaction coordinate' that connects the liquid to the crystalline phase. We find that the bond-orientational order parameter Q_6 [Eq. (8)] is a suitable reaction coordinate, as it satisfies the following criteria:

(1) It is invariant under any global rotation of an isolated crystallite with respect to the simulation box.

(2) It is large for *all* crystalline structures of interest and vanishes in the isotropic fluid phase (at least, in the thermodynamic limit).

(3) It is relatively cheap to compute.

Umbrella sampling[37] is used to measure the Gibbs free-energy barrier as a function of Q_6. The structure of the resulting phases is analyzed using a number of different techniques. As an illustration, we applied the method to study the transition region between crystal and liquid in a simple model system, namely, an assembly of r^{-12}-soft spheres. We find that at, or near, the point where the fluid phase is known to coexist with the (stable) fcc solid, a gradual increase of Q_6 leads to the formation of an imperfect bcc phase. The transformation from liquid to bcc crystal is found to proceed with little hysteresis. In contrast, the transformation of an fcc crystal to the isotropic fluid requires a much higher activation energy and then proceeds irreversibly. We have never been able to transform the liquid into an fcc crystal. Our analysis of a number of different order parameters in both the liquid and the crystalline state, suggests that bcc-like fluctuations are already present in the liquid phase. This observation is in agreement with the results of previous molecular dynamics simulations of the same system.[18,19]

We have also performed simulations of the same system at moderate supercooling. In that case we find that the free-energy barrier towards the formation of bcc crystallites has disappeared altogether in small systems ($N = 125$) and is quite small in a larger system ($N = 1000$). As before, fcc crystallites are never formed from the liquid. This suggests that the free-energy barrier between the liquid and the latter crystal phase remains appreciable.

One of the most striking observations in this study of the free-energy barrier to crystal formation is that, although fcc is presumably the stable solid phase, the metastable bcc phase is the one that can be reached without crossing a high free-energy barrier. Of course, our simulations only provide information about the statics of crystal nucleation. We cannot rule out the possibility that the 'reactive flux' over the high barrier to the fcc phase is larger than that over the low barrier to the bcc phase. However, as was discussed in the Sec. I, computer-simulation studies of the dynamics of crystal nucleation in the r^{-12}-soft-sphere system[19,18] reveal that the (metastable) bcc phase forms more readily than the fcc phase, even at large supercooling. Tanemura *et al.*[18] have suggested that the effect of the periodic boundary condition is to exert a stress on growing nuclei that eventually transforms fcc crystallites into a bcc form. If this explanation were correct, we would expect to see no bcc crystallites in homogeneous nucleation studies of large model systems. However, as shown in a simulation by Cape *et al.*[19] on a 4000-particle r^{-12} system, bcc nuclei still form and grow in a relatively large system. On basis of the present simulations, it seems more likely that bcc crystallites nucleate more easily, simply because the free-energy barrier for nucleation of this phase is low. In this context it is worth pointing out that the original Alexander–McTague theory[31] in which it is argued that bcc nuclei should be favored in weakly first-order phase transitions, is also based on static, rather than dynamic considerations.

We stress once more that the free-energy barriers measured in simulations of small, periodic systems may differ from the 'true' barriers for homogeneous nucleation. In order to measure the true free energy barriers for crystal nucleation, we would have to perform simulations on much larger systems [$\mathcal{O}(10^4)$] particles, at finite supercooling. In the present study we have not attempted to estimate the

height of the nucleation barriers in systems of more than 10^3 particles. However, none of the techniques described above are limited to small systems. In any event, we think that our consistent observation of a low free-energy barrier between the liquid and the bcc phase is meaningful, even if the absolute barrier height is not.

It would be interesting to apply the method that we have presented to systems containing $\mathcal{O}(10^4)$ particles. This would provide an opportunity to study the formation of separate crystal nuclei at moderate supercooling, in a controlled manner. One obvious model system to study in such a large-scale simulation would be the Lennard-Jones system. In that case there is overwhelming evidence that crystallization at large supercooling starts with the formation of fcc nuclei.[16] It would be very interesting to see if the relative height of the barriers to nucleate fcc and bcc crystallites changes as the degree of supercooling is reduced. This would make it possible to test the Alexander–McTague conjecture[31] in the temperature range where it is supposed to apply. We recall that direct simulation of crystal nucleation at moderate supercooling is extremely time consuming.

Finally, we note that the present scheme can be used as a starting point to compute the rate of crystal nucleation, using the approach described in Ref. 34.

ACKNOWLEDGMENTS

One of us (J. V. D.) gratefully acknowledges the hospitality of the FOM Institute during the period in which this work was carried out. The work of the FOM Institute is part of the research programme of FOM (Stichting Fundamenteel Onderzoek der Materie) and is supported by the Nederlandse Organisatie voor Wetenschappelijk Onderzoek (NWO). We gratefully acknowledge several stimulating discussions with Henk Lekkerkerker. D. F. thanks Ali Alavi for a critical reading of the manuscript.

[1] B. J. Alder and T. E. Wainwright, J. Chem. Phys. **27**, 1208 (1957).
[2] W. W. Wood and J. D. Jacobson, J. Chem. Phys. **27**, 1207 (1957).
[3] W. G. Hoover and F. H. Ree, J. Chem. Phys. **47**, 4873 (1967).
[4] J. P. Hansen and L. Verlet, Phys. Rev. **184**, 151 (1969).
[5] W. G. Hoover, S. G. Gray, and K. W. Johnson, J. Chem. Phys. **55**, 1128 (1971).
[6] E. J. Meijer and D. Frenkel, J. Chem. Phys. **94**, 2269 (1991).
[7] W. G. Hoover, D. A. Young, and R. Grover, J. Chem. Phys. **56**, 2207 (1972).
[8] M. J. Mandell, J. P. McTague, and A. Rahman, J. Chem. Phys. **64**, 3699 (1976).
[9] M. J. Mandell, J. P. McTague, and A. Rahman, J. Chem. Phys. **64**, 3070 (1977).
[10] C. S. Hsu and A. Rahman, J. Chem. Phys. **71**, 4974 (1979).
[11] R. D. Mountain and P. K. Basu, J. Chem. Phys. **78**, 7318 (1983).
[12] J. D. Honeycutt and H. C. Andersen, Chem. Phys. Lett. **108**, 535 (1984).
[13] J. D. Honeycutt and H. C. Andersen, J. Phys. Chem. **90**, 1585 (1986).
[14] S. Nosé and F. Yonezawa, J. Chem. Phys. **84**, 1803 (1986).
[15] J. Yang, H. Gould, and W. Klein, Phys. Rev. Lett. **60**, 2665 (1988).
[16] W. C. Swope and H. C. Andersen, Phys. Rev. B **41**, 7042 (1990).
[17] Y. Hiwatari, H. Matsuda, T. Ogawa, N. Ogita, and A. Ueda, Progr. Theor. Phys. **52**, 1105 (1974).
[18] M. Tanemura, Y. Hiwatari, H. Matsuda, T. Ogawa, N. Ogita, and A. Ueda, Progr. Theor. Phys. **58**, 1079 (1977).
[19] J. N. Cape, J. L. Finney, and L. V. Woodcock, J. Chem. Phys. **75**, 2366 (1981).
[20] R. D. Mountain and A. C. Brown, J. Chem. Phys. **80**, 2730 (1984).
[21] M. O. Robbins, K. Kremer, and G. S. Grest, J. Chem. Phys. **88**, 3286 (1988).
[22] N. Pistoor and K. Kremer, Progr. Colloid Polym. Sci. **81**, 184 (1990).
[23] M. S. Watanabe and K. Tsumuraya, J. Chem. Phys. **87**, 4891 (1987).
[24] C. S. Hsu and A. Rahman, J. Chem. Phys. **70**, 5234 (1979).
[25] D. Frenkel and J. P. McTague, Annu. Rev. Phys. Chem. **31**, 491 (1980).
[26] D. W. Oxtoby, Adv. Chem. Phys. **70**, 263 (1988).
[27] J. H. R. Clarke, J. Chem. Soc. Faraday Trans. II **75**, 1371 (1979).
[28] C. Smits, J. S. van Duijneveldt, J. K. G. Dhont, H. N. W. Lekkerkerker, and W. J. Briels, Phase Trans. **21**, 157 (1990).
[29] W. Ostwald, Z. Phys. Chem. **22**, 289 (1897).
[30] I. N. Stranski and D. Totomanow, Z. Physikal. Chem. **163**, 399 (1933).
[31] S. Alexander and J. P. McTague, Phys. Rev. Lett. **41**, 702 (1978).
[32] W. Klein and F. Leyvraz, Phys. Rev. Lett. **57**, 2845 (1986).
[33] R. E. Cech, J. Metals **8**, AIME Trans. **206**, 585 (1956).
[34] D. Chandler, J. Chem. Phys. **68**, 2959 (1978).
[35] E. A. Carter, G. Ciccotti, J. T. Hynes, and R. Kapral, Chem. Phys. Lett. **156**, 472 (1989). For a recent review, see G. Ciccotti, in *Computer Simulation in Materials Science*, edited by M. Meyer and V. Pontikis (Kluwer, Dordrecht, 1991), p. 119.
[36] L. D. Landau and E. M. Lifshitz, *Statistical Physics*, 3rd ed. (Pergamon, London, 1980).
[37] G. M. Torrie and J. P. Valleau, Chem. Phys. Lett. **28**, 578 (1974).
[38] P. J. Steinhardt, D. R. Nelson, and M. Ronchetti, Phys. Rev. B **28**, 784 (1983).
[39] A. R. Edmonds, *Angular Momentum in Quantum Mechanics* (Princeton University, Princeton, 1974).
[40] R. Eppenga and D. Frenkel, Mol. Phys. **52**, 1303 (1984).
[41] D. J. Adams, CCP5 Quarterly **10**, 30 (1983).
[42] H. Ogura, H. Matsuda, T. Ogawa, N. Ogita, and A. Ueda, Prog. Theor. Phys. **58**, 419 (1977).
[43] M. P. Allen and D. J. Tildesley, *Computer Simulation of Liquids* (Clarendon, Oxford, 1989).
[44] D. Frenkel, R. J. Vos, C. G. de Kruif, and A. Vrij, J. Chem. Phys. **84**, 4625 (1986).
[45] K. Binder, Phys. Rev A **25**, 1699 (1982).
[46] W. G. Hoover, M. Ross, K. W. Johnson, D. Henderson, J. A. Barker, and B. C. Brown, J. Chem. Phys. **52**, 4931 (1970).